Computer Assisted Mechanics and Engineering Sciences, 10: 57–68, 2003.

Numerical simulation of heat and mass transfer in composite fluid–porous layer with transverse magnetic field

R. Younsi[1], A. Harkati[2] and D. Kalache[1]
[1] *Fluid Mechanics Laboratory, Physics Institute, USTHB*
B.P. 32, El-Alia, 16111 Algiers, Algeria
[2] *Theoretical Physics Laboratory, Physics Institute, USTHB*
B.P. 32, El-Alia, 16111 Algiers, Algeria

(Received January 2, 2001)

The aim of this paper is to simulate numerically the two-dimensional steady state double diffusive flow in a composite fluid–porous layer, submitted to a transverse magnetic field. Both the temperature and solute gradients are imposed horizontally, and the two-buoyancy effects can either augment or counteract each other. The Darcy equation, including Brinkman and Forchheimer terms to account for viscous and inertia effects, respectively is used for the momentum equation, and the SIMPLER algorithm, based on finite volume approach is used to solve the pressure–velocity coupling. An extensive series of numerical simulations is conducted in the range: $Ra = 10^5$, $10^{-8} \leq Da \leq 1$, $N = 1$, $Le = 10$ and $0 \leq Ha \leq 10^2$. This study is limited to $Pr = 7$ for the binary solution of (Na_2Co_3). This choice is motivated by the experimental work on phase change realized in laboratory. It is shown that the main effect of the porous layer is to reduce the heat and mass transfer when the permeability is reduced. Isotherms and streamlines are plotted for several values of Hartman (Ha), Darcy number (Da) and porous layer thickness (Xp). The effect of the magnetic field is found to be rather significant on the flow pattern, heat and mass transfer.

Keywords: double diffusion, porous media, magneto-hydrodynamics, finite volume method

NOMENCLATURE

A – aspect ratio $= H/L$
$\vec{B}$ – magnetic field
C_p – specific heat at constant pressure, J/Kg · K
C_f – inertial coefficient
D – mass diffusivity, m^2s^{-1}
Da – Darcy number $= K/H^2$
$\vec{g}$ – acceleration due to gravity
H – cavity high, m
Ha – Hartman number $= B\varepsilon(\sigma H/\nu)^{1/2}$
k – thermal conductivity, W/m · K
K – permeability, m^2
L – cavity width, m
Le – Lewis number $= Sc/Pr$
N – buoyancy ratio $= Gr_s/Gr_t$
Nu_0 – overall Nusselt number
P – pressure, Pa
Pr – Prandtl number $= \nu/\alpha$
Ra_t – Rayleigh number $= Gr_t \cdot Pr$

Sc – Schmidt number $= \nu/D$
Sh_0 – overall Sherwood number
$U(V)$ – dimensionless velocity in $X(Y)$ direction
$\mathbf{V}$ – velocity vector
Gr_t – thermal Grashof number $= g\beta_t \Delta T H^3/\nu^2$
Gr_s – solutal Grashof number $= g\beta_c \Delta C H^3/\nu^2$
(X, Y) – dimensionless Cartesian coordinate

Greek Symbols

α – thermal diffusivity, $\mathrm{m^2 s^{-1}}$
β_t – coefficient of thermal expansion of fluid
β_s – coefficient of solutal expansion of fluid
ρ – density, $\mathrm{kg} \cdot \mathrm{m^{-3}}$
ν – kinematic viscosity, $\mathrm{m^2 s^{-1}}$
τ – dimensionless time
Θ – dimensionless temperature $= (T - (T_1 + T_2)/2)/\Delta T$
Φ – dimensionless concentration $= (C - (C1 + C2)/2)/\Delta C$
ΔT – temperature difference $= T_1 - T_2$
ΔC – concentration difference $= C_1 - C_2$
ε – porous media porosity
Ψ – stream function

Subscripts

1 – heated surface
2 – cooled surface
f – fluid
p – porous media
0 – average value

Superscripts

i – time iteration

1. Introduction

Electromagnetic field has been used in the metal industry to control microstructures solidification and to reduce or eliminate natural convection in the melt. The magnetic fields give rise to extra forced flows in the melt, enhancing in such a way the significance of the convective phenomena. The double-diffusive natural convection in a fluid saturated porous medium occurs in a wide variety of applications such as geothermal energy, fibrous insulating materials, cryogenic systems, etc. the combined heat and mass transfer in porous media is limited, because of complexities involved in double-diffusive natural convection. Most of previous studies in this topic use Darcy's law for solving flow within the porous medium [11]. Natural convection of heat and mass transfer in a square porous cavity subjected to constant temperature and concentration has been investigated by Trevisan and Bejan [11]. The authors use the Darcy's model for modeling the flow in porous medium. The numerical study has been carried out for a given range of Darcy–Rayleigh number, Lewis number and buoyancy ratio. Our study focuses on combined thermal and solutal natural convection of a binary fluid in a closure with thin porous layer on the left wall and submitted to a transverse magnetic field. Such configuration has been previously considered in the case of thermal convection

by Le Breton et al. [8]. These studies shown that the main effect of porous medium is to reduce the upwind flow and then to decrease the convective heat transfer. Lage [5] studied the effect of the convective inertia term on Bénard convection in porous medium. The author shows that inertia term included in the general momentum equations has no effect on the overall heat transfer. Bian et al. [1] consider the interaction of an external magnetic field with convection currents in porous medium. The porous medium was modeled according to Darcy' s model. It is found that the application of a magnetic field, modifies the temperature and fields significantly. The aim of this paper is to analyze the effect of magnetic field for the double diffusion natural convection flow in the presence of a porous layer. The flow is modeled using the generalized model of Darcy–Brinkman–Forchheimer. The effect of permeability and porous layer thickness are also presented.

2. Problem definition and governing equations

The problem considered is a two-dimensional natural convection flow in a vertical square cavity filled with a binary fluid, see Fig. 1. Horizontal temperature and concentration differences are considered between the vertical walls, and zero mass and heat flux are imposed at the horizontal walls. A uniform magnetic field is applied transversally. Both velocity components are equal to zero on boundaries. The left vertical wall is covered with thin porous layer. For simpler analysis, some assumptions are made:

- The binary fluid is assumed to be Newtonian incompressible and to satisfy the Boussinesq approximation.
- The flow in the cavity is laminar and two-dimensional.
- The porous medium is supposed to be isotropic homogeneous and in thermodynamic equilibrium with the binary fluid.
- The Soret and Dufour effects are neglected.
- The Reynolds magnetic number of the fluid is neglected.

The density variations upon temperature and concentration are described by the state equation

$$\rho = \rho_0 \left[1 - \beta_T (T - T_0) - \beta_C (C - C_0)\right]$$

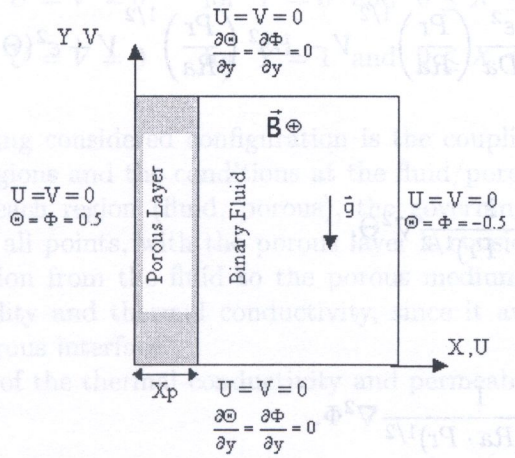

Fig. 1. The physical model and coordinate system

where

$$\beta_T = -\frac{1}{\rho}\left[\frac{\partial \rho}{\partial T}\right]_C \quad \text{and} \quad \beta_C = -\frac{1}{\rho}\left[\frac{\partial \rho}{\partial C}\right]_T.$$

Then, applying the theorem of conservation and introducing the dimensionless parameters as given below [5],

$$(X,Y) = \frac{(x,y)}{H}, \qquad (U,V) = \frac{(u,v)}{(\alpha_p/H)(Ra \cdot Pr)^{1/2}},$$

$$\tau = \frac{t}{(H^2/\alpha_p)}(Ra \cdot Pr)^{1/2}, \qquad \lambda = \frac{(\rho C_p)_p}{(\rho C_p)_f},$$

$$\Theta = \frac{T - (T_1 + T_2)/2}{T_1 - T_2}, \qquad \Phi = \frac{C - (C_1 + C_2)/2}{C_1 - C_2}, \qquad P = \frac{\varepsilon^2 H^2 (p)}{\rho_f \alpha_p^2 (Ra \cdot Pr)}.$$

The definition of all variables is given in Nomenclature.

We obtain the following dimensionless governing equations as given also by Lage [5]:

– *Continuity equation*:

$$\frac{\partial U}{\partial X} + \frac{\partial V}{\partial Y} = 0, \tag{1}$$

– *X-momentum equation*:

$$\frac{1}{\varepsilon}\frac{\partial U}{\partial \tau} + (\mathbf{V} \cdot \boldsymbol{\nabla})U = -\frac{\partial P}{\partial X} + \varepsilon \left(\frac{Pr}{Ra}\right)^{1/2} \nabla^2 U - \frac{C_f \varepsilon^2}{\sqrt{Da}} |\mathbf{V}| U - \frac{\varepsilon^2}{Da}\left(\frac{Pr}{Ra}\right)^{1/2} U - Ha^2 \left(\frac{Pr}{Ra}\right)^{1/2} U, \tag{2}$$

– *Y-momentum equation*:

$$\frac{1}{\varepsilon}\frac{\partial V}{\partial \tau} + (\mathbf{V} \cdot \boldsymbol{\nabla})V = -\frac{\partial P}{\partial Y} + \varepsilon \left(\frac{Pr}{Ra}\right)^{1/2} \nabla^2 V - \frac{C_f \varepsilon^2}{\sqrt{Da}} |\mathbf{V}| V - \frac{\varepsilon^2}{Da}\left(\frac{Pr}{Ra}\right)^{1/2} V - Ha^2 \left(\frac{Pr}{Ra}\right)^{1/2} V + \varepsilon^2 (\Theta + N\Phi), \tag{3}$$

– *Energy equation:*

$$\frac{1}{\lambda}\frac{\partial \Theta}{\partial \tau} + (\mathbf{V} \cdot \nabla)\Theta = \frac{1}{(Ra \cdot Pr)^{1/2}} \nabla^2 \Theta, \tag{4}$$

– and *Species equation*:

$$\varepsilon \frac{\partial \Phi}{\partial \tau} + (\mathbf{V} \cdot \nabla)\Phi = \frac{1}{Le \cdot (Ra \cdot Pr)^{1/2}} \nabla^2 \Phi. \tag{5}$$

All the dimensionless parameters are given in the Nomenclature.

The momentum equation is a balance among:

$\left(\frac{1}{\varepsilon}\frac{\partial V}{\partial \tau} + (\mathbf{V}\cdot\nabla)V\right)$ – macroscopic inertia force or macroflow development term,

$\frac{\partial P}{\partial Y}$ – pressure gradient,

$\varepsilon\left(\frac{Pr}{Ra}\right)^{1/2}\nabla^2 V$ – macroscopic or bulk viscous shear stress diffusion, also called Brinkman viscous term,

$\frac{C_f\varepsilon^2}{\sqrt{Da}}|\mathbf{V}|V$ – Forchheimer term, also called Ergun inertial term,

$\frac{\varepsilon^2}{Da}\left(\frac{Pr}{Ra}\right)^{1/2}V$ – microscopic viscous shear stress: Darcy term,

$Ha^2\left(\frac{Pr}{Ra}\right)^{1/2}V$ – electromagnetic force,

$\varepsilon^2(\Theta + N\Phi)$ – buoyancy term.

The Brinkman term is added in order to obtain the classical Navier–Stokes equations when the Darcy number becomes high to account for the boundary layer in the porous medium.

When the flow field is significant, the non-linear inertial effects become very significant. Ward(1961) has proposed to add the Forchheimer term, which is a drag term in the momentum equation.

The initial and boundary conditions for the dimensionless equations are as follows:

– *Initial condition* (at $\tau = 0$),

$$\begin{cases} \Theta = \Theta_0 = 0, \\ \Phi = \Phi_0 = 0, \\ U = V = 0, \end{cases} \quad \text{for } 0 \le Y \le 1 \text{ and } 0 \le X \le 1/A, \tag{6}$$

– *Boundary conditions*,

$$\begin{cases} \Theta = \Phi = 0.5, & U = V = 0 & \text{for } X = 0 \text{ and } 0 \le Y \le 1, \\ \Theta = \Phi = -0.5, & U = V = 0 & \text{for } X = 1/A \text{ and } 0 \le Y \le 1, \\ \dfrac{\partial\Theta}{\partial Y} = \dfrac{\partial\Phi}{\partial Y} = 0, & U = V = 0 & \text{for } Y = 0 \text{ and } 0 \le X \le 1/A, \\ \dfrac{\partial\Theta}{\partial Y} = \dfrac{\partial\Phi}{\partial Y} = 0, & U = V = 0 & \text{for } Y = 1 \text{ and } 0 \le X \le 1/A. \end{cases} \tag{7}$$

The problem in modeling considered configuration is the coupling of the momentum equation in the fluid and porous regions and the conditions at the fluid/porous interface. Instead of solving one set of equations for each region (fluid, porous), the governing equation could be combined into a unique set valid at all points, with the porous layer is considered as a pseudo-fluid. In this representation the transition from the fluid to the porous medium is achieved through a spatial variation of the permeability and thermal conductivity, since it avoids explicitly considering the conditions at the fluid–porous interface.

The variation in space of the thermal conductivity and permeability are written in dimensional form as follows,

$$k(X,Y) = k_f\,, \quad K(X,Y) = \infty\,, \quad \text{for} \quad Xp < X < 1/A\,, \tag{8}$$

$$k(X,Y) = k_P\,, \quad K(X,Y) = K_P\,, \quad \text{for} \quad 0 < X < Xp\,, \tag{9}$$

where $k(X,Y)$ is the thermal conductivity and $K(X,Y)$ is the permeability.

With conditions of Eqs. (8) and (9), in the porous layer the permeability exists ($1/Da \neq 0$).

In the fluid region the permeability disappears ($Da = K_P/H^2 \to \infty \Rightarrow 1/Da = 0$) and we obtain the classical Navier–Stokes equations without porous medium.

With the use of this technique, the conditions at the fluid/porous layer interface are automatically satisfied; thus the numerical solution procedure is greatly simplified.

Note that it is not necessary to explicitly use the dimensional value (ex. permeability K_P) in subsequent computations, because it appears through the dimensionless parameters ($Da = K_P/H^2$).

3. Numerical procedure

The coupled transient equations are solved to obtain a steady state solution. When a convergent result is approached, the transient terms vanish and the steady-state equations are solved. This formulation more over allows us to detect instabilities [8].

The differential equations are discretised in space with the control-volume finite difference method described by Patankar [10]. The resulting finite difference scheme has the form

$$A_P\phi_P = A_N\phi_N + A_S\phi_S + A_E\phi_E + A_W\phi_W + b. \tag{10}$$

Expressions for the coefficients in Eq. (10) may be found in [10]. The advection-diffusion part of the coefficients A_N, A_S, A_E and A_W is modified for stability according to the power law scheme of [10]. The source term b includes the values of at previous time step. The discretisation technique is well known and a detailed description is not needed. The linear system derived from the conservation equations are solved using line-by-line method. As the momentum equation is formulated in terms of the primitive variables (U, V, P) the iterative procedure includes a pressure correction calculation method to solve the pressure–velocity coupling (the Simpler technique [10]). The simulation are generally performed using 81×81 sinusoidal grid. It is realized that this relatively course grid is adequate to resolve all details of the flow structures in the cavity. The selected mesh size should only be viewed as a compromise between accuracy and computational time. The calculations were performed on PC 700 MHz. The convergence of the numerical solution was monitored locally. The max-norm was used for the velocity components U, V, temperature and concentration. The convergence criterion at each time step is

$$\max \left| \frac{(U,V,\Theta,\Phi)^{i+1} - (U,V,\Theta,\Phi)^{i}}{(U,V,\Theta,\Phi)^{i}} \right| \leq 10^{-4}, \tag{11}$$

in which i and $i+1$ denote two consecutive iterations at the same time step.

The average heat and mass transfer at the walls are given in dimensionless terms by the Nusselt and Sherwood numbers defined as follows,

$$Nu_0 = \int_0^1 \left[\frac{\partial\Theta}{\partial X}\right]_{X=0} \mathrm{d}Y, \qquad Sh_0 = \int_0^1 \left[\frac{\partial\Phi}{\partial X}\right]_{X=0} \mathrm{d}Y, \tag{12}$$

4. Test validation

The numerical accuracy of the present study has been checked over a large number of purely thermal convection in a fully porous cavity ($Xp = 1$), the results has been compared with the results of earlier studies in Tables 1 and 2, for the Darcy and combined Darcy–Brinkman representation of the porous medium flow. The validation is performed using 81×81 sinusoidal grid. It may be seen from the results, that the agreement with [7, 9] is excellent in most cases. Indeed, our results present a difference less than 2% in comparison with Nithiarasu [9] results. As an additional check on the numerical accuracy, the present study has been compared for purely thermal natural convection

Table 1. Darcy model (pure heat transfer, $N = 0$)

$Ra^* = Ra_t \cdot Da$	$\overline{Nu}$			
	Lauriat et al. [7]	Trevisan et al. [11]	Nithiarasu et al. [9]	Present work
10	1.07		1.08	1.06
50		2.02	1.958	1.936
100	3.09	3.27	3.02	2.98
500			8.38	8.32
1000	13.41	18.38	12.514	12.49

Table 2. Darcy–Brinkman model (pure heat transfer, $Pr = 1$)

$Ra^* = Ra_t \cdot Da$	Da	$\overline{Nu}$		
		Lauriat et al. [7]	Nithiarasu et al. [9]	Present work
10	10^{-6}	1.07	1.08	1.06
100	10^{-6}	3.06	3.00	2.98
1000	10^{-6}	13.2	12.25	12.11
10	10^{-2}	1.02	1.02	0.99
100	10^{-2}	1.7	1.71	1.68
1000	10^{-2}	4.26	4.26	4.24

Table 3. Darcy model (pure heat transfer, $N = 0$)

$Ra^* = Ra_t \cdot Da$	$\overline{Nu}$		
	Lauriat et al. [6]	Goyeau et al. [2]	Present work
100	2.08	2.08	2.06
200	3.03	3.04	2.99
500	4.92	4.94	4.89
1000	7.02	7.05	7.01

($N = 0$) and $Le = 100$, in a porous cavity ($Xp = 1$). In the absence of concentration-driven convection ($N = 0$), there is still buoyancy due to temperature differences. Table 3 shows the comparison, and the agreement is seen to be excellent [2], difference is less than 1%.

5. Results and discussion

Due to large number of parameters and for brevity, only selected results are presented for the case of a cavity with aspect ratio unity ($A = 1$) and the Prandtl number of the binary solution (Na_2Co_3) $Pr = 7$. The ranges of parameters that have been examined in this study are the Hartman number $0 \leq Ha \leq 10^2$, the Darcy number $10^{-8} \leq Da \leq 1$, and thickness of the porous layer $0 \leq Xp \leq 1$. The conductivity ratio is $\lambda = 1$ and the representative porosity is fixed at $\varepsilon = 0.7$ for the porous medium. The inertia parameter C_f is calculated using the Ergun [3] model,

$$C_f = \frac{1.75}{(150\varepsilon^3)^2},$$

which means that in the present case $C_f = 0.25$.

5.1. Influence of Hartman number

Figure 2 illustrates typical streamlines, velocity vectors, isotherms and concentration lines for $Ra = 10^5$, $Da = 10^{-5}$, $Pr = 7$, $Le = 10$, $N = 1$, and $Ha = 10$, 60 and 100, respectively. The influence of a magnetic field is apparent from this figure. Figure 2a shows the results obtained for $Ha = 0$ "absence of magnetic field". The flow, Isotherms and isoconcentrations are similar to those obtained by other investigators (see Kimura and Bejan [4]). The resulting flow regime is characterized by a boundary layer of constant thickness. Also, the parallelism of the flow and the existence of linear thermal and solutal stratification are clearly illustrated. Due to the thermal and solutal boundary conditions considered here, the bottom wall has a higher temperature and concentration as the top inclined wall. As a result, the direction of the flow is counterclockwise. When the magnetic field is applied, the flow recalculation is progressively inhibited by the retarding effect of the electromagnetic body force (Figs. 2b,c). The maxima of stream function values are $\Psi_{max} = 9.43 \cdot 10^{-3}$ for $Ha = 0$, $\Psi_{max} = 1.63 \cdot 10^{-3}$ for $Ha = 60$ and $\Psi_{max} = 8.25 \cdot 10^{-4}$ for $Ha = 100$. From the study of Bian et al. [1], it appears that the value of Hartman for which the natural convection is fully inhibited decreases with decreasing the Prandtl number. For $Pr \ll 1$, high value of the conductivity of metals dominates heat transfer.

More quantitative comparison are presented here in terms of V-velocity, temperature and solute profiles. All the profiles are plotted along the middle horizontal line of the enclosure, i.e., along the line of $Y = 0.5$. Figures 3 and 4 compare profiles obtained for $Da = 10^{-2}$ and $Da = 10^{-5}$ at different Hartman number $Ha = 0$, 20, 40 and 60. The effect of Hartman number on the convection field is well reflected by the progressive reduction of the velocity, temperature and solute concentration gradients as the Hartman number is increased. It appears that for moderate value of Darcy number ($Da = 10^{-2}$), as the Hartman increases, the flow field, temperature and concentration are slightly influenced in both porous and fluid regions. For low value of Darcy number ($Da = 10^{-5}$), corresponding to low permeability, as Hartman number increases the flow field, temperature and concentration are inhibited only in the fluid region, because the porous medium acts as a solid wall.

Another view of the effect of Hartman on heat and mass transfer is found in Fig. 5, where Nusselt and Sherwood numbers are plotted as a function of Ha. The analysis of this figure indicates that for small values of Ha, the boundary layer regime prevails. As the Hartman number increases, the electromagnetic body force increases which suppresses progressively the strength of the convective motion, and thus boundary layer regime is followed by the double diffusive regime for which Nusselt and Sherwood numbers tend to one.

a) $Ha = 0$

b) $Ha = 60$

c) $Ha = 100$

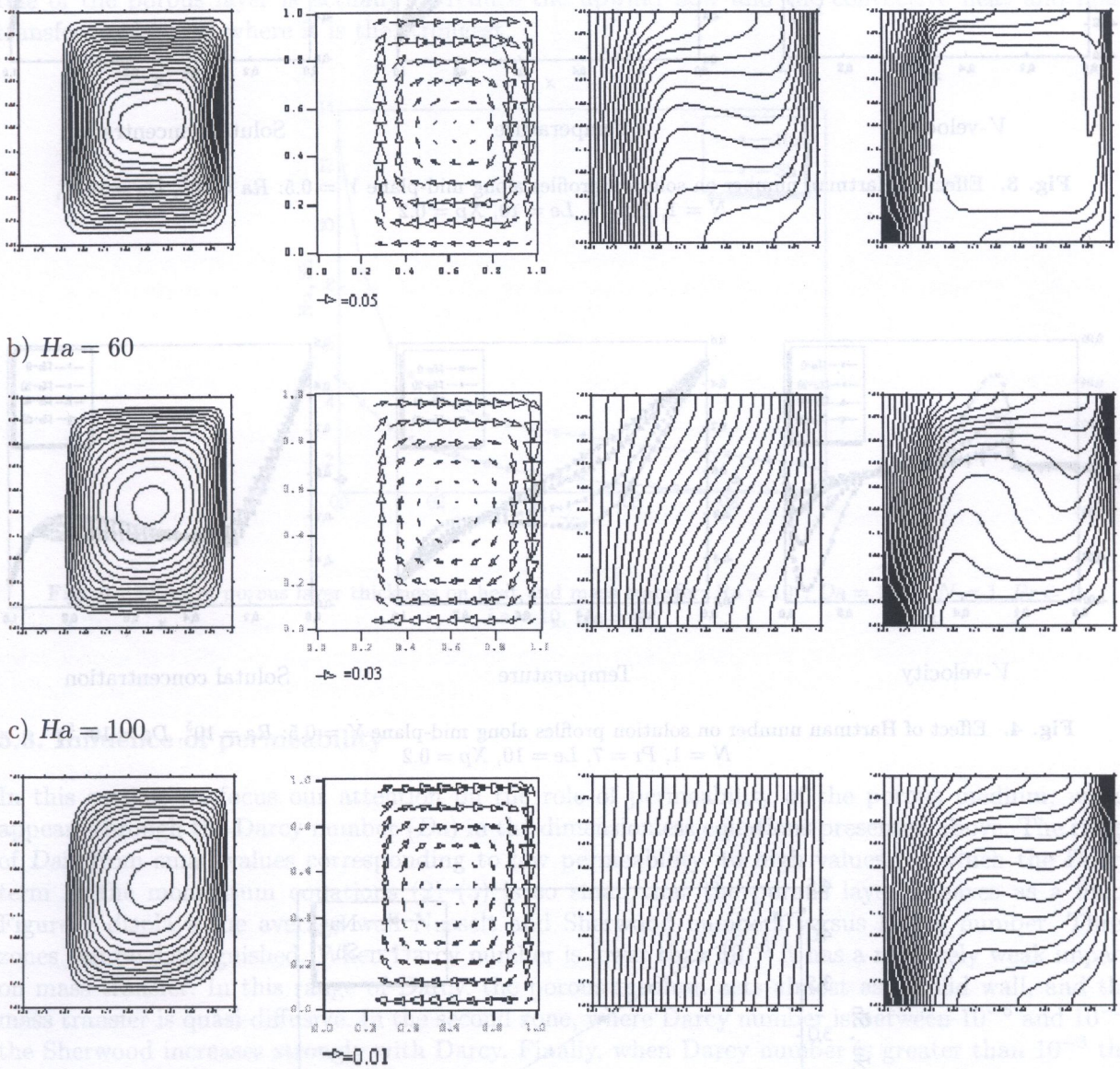

Fig. 2. Streamlines, isotherms, and isoconcentrations versus Hartman number: $Ra = 105$, $Da = 10^{-5}$, $N = 1$, $Pr = 7$, $Le = 10$, $Xp = 0.2$

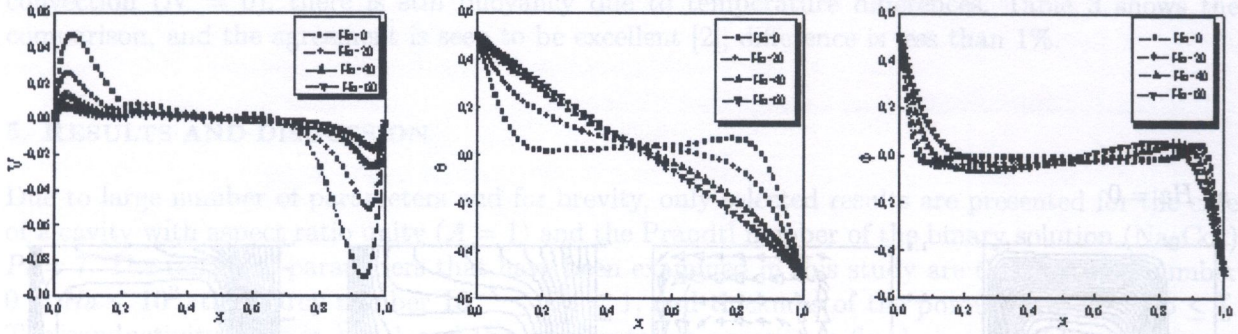

V-velocity Temperature Solutal concentration

Fig. 3. Effect of Hartman number on solution profiles along mid-plane $Y = 0.5$: $Ra = 10^5$, $Da = 10^{-2}$, $N = 1$, $Pr = 7$, $Le = 10$, $Xp = 0.2$

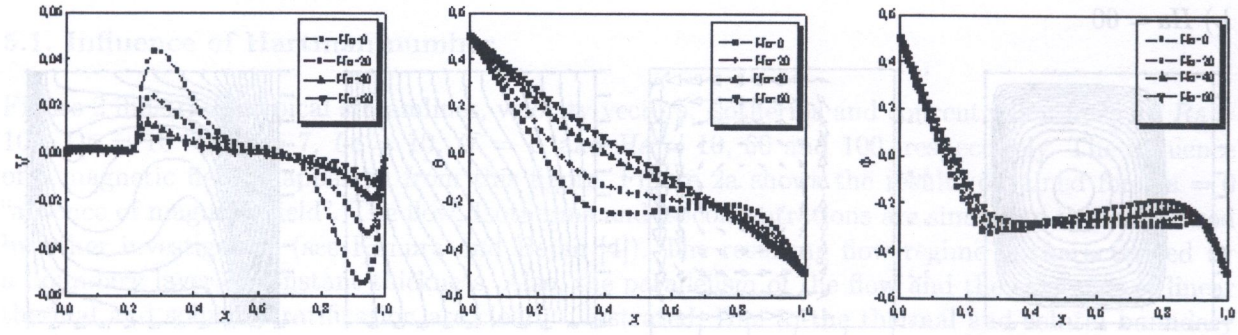

V-velocity Temperature Solutal concentration

Fig. 4. Effect of Hartman number on solution profiles along mid-plane $Y = 0.5$: $Ra = 10^5$, $Da = 10^{-5}$, $N = 1$, $Pr = 7$, $Le = 10$, $Xp = 0.2$

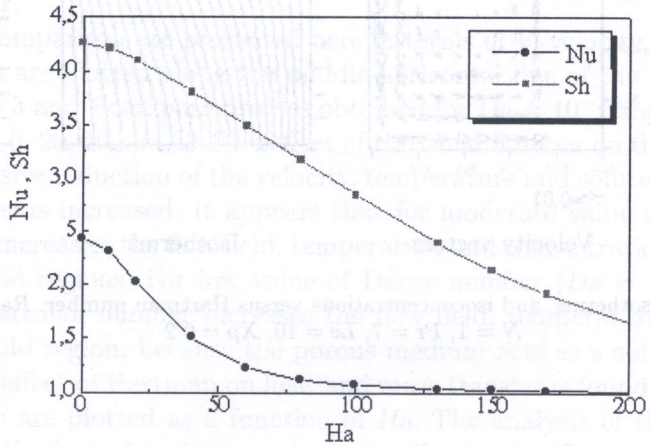

Fig. 5. Effect of Hartman number on the Nusselt and Sherwood numbers: $Ra = 10^5$, $Da = 10^{-5}$, $N = 1$, $Pr = 7$, $Le = 10$, $Xp = 0.2$

5.2. Influence of porous layer thickness

The set of simulation results displayed in Fig. 6 shows the variation of the average Nusselt and Sherwood numbers in a vertical plan as a function of Xp, for Ra=10^5, Da=10^{-5}, Le=10, and N=1. The figure shows that it is not necessary to introduce a very high thickness porous medium to obtain a significant decrease of the heat and mass transfer. For a thickness value greater than 0.305, the Nusselt and Sherwood numbers decrease very slowly for an increasing thickness. This observation is in good agreement with the result reported by Le Breton and al. [8]. It can be deduced that the role of the porous layer is actually to reduce the upwind flow and the convective heat and mass transfer in the area where it is the strongest.

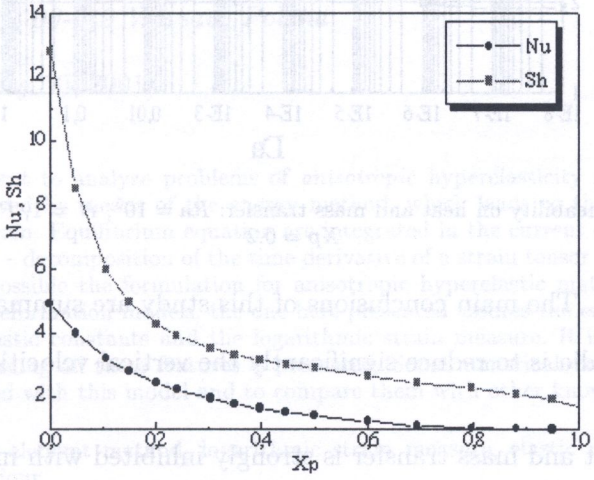

Fig. 6. Effect of porous layer thickness on heat and mass transfer: $Ra = 10^5$, $Da = 10^{-5}$, $N = 1$, $Pr = 7$, $Le = 10$, $Ha = 0$

5.3. Influence of permeability

In this section we focus our attention on the role of permeability of the porous medium, which appears through the Darcy number (Da) in the dimensionless equations presented above. The range of $Da$is from small values corresponding to low permeability, to high values for which the Darcy term in the momentum equations (2)–(3) is so small that the porous layer behaves as a fluid. Figure 7 displays the average wall Nusselt and Sherwood numbers versus Darcy number. Three zones can be distinguished. When Darcy number is lower than 10^{-6} it has a relatively weak impact on mass transfer. In this range of Darcy, the porous medium acts almost as a solid wall, and the mass transfer is quasi-diffusive. In the second zone, where Darcy number is between 10^{-6} and 10^{-3}, the Sherwood increases strongly with Darcy. Finally, when Darcy number is greater than 10^{-3} the Sherwood number remains nearly constant.

The variation of Nusselt number with Darcy number is approximately the same as observed for as the Sherwood number. The main difference is that this variation is not monotonic and exhibits a significant minimum. The increase of permeability results in a better penetration of the flow in the porous layer and finally in the enhancement of the overall heat transfer.

6. Conclusion

Double-diffusive natural convection in composite fluid–porous layer in the presence of a magnetic field has been studied numerically. The results obtained are in good agreement with the heat transfer

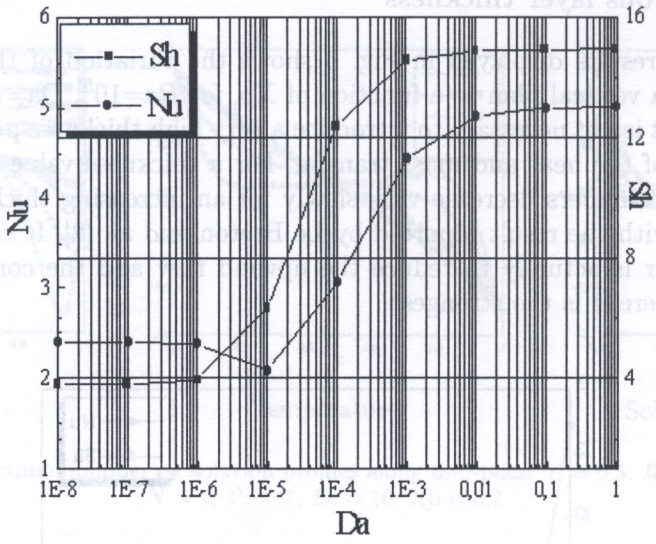

Fig. 7. Effect of permeability on heat and mass transfer: $Ra = 10^5$, $N = 1$, $Pr = 7$, $Le = 10$, $Ha = 0$, $Xp = 0.2$

results given in literature. The main conclusions of this study are summarized here:

- The role of porous media is to reduce significantly the vertical velocities that occur in boundary layer.
- The convection of heat and mass transfer is strongly inhibited with increasing magnetic field.
- The overall heat and mass transfers decrease for a decreasing permeability.

The present analysis is focused on the influence of a limited number of dimensionless parameters. As an extension of this work, it is particularly relevant to take into account the effect of aspect ratio (A), the Prandtl number (Pr), the conductivity ratio (λ), and correlate heat and mass transfer.

References

[1] W. Bian, P. Vasseur, E. Bilgen, F. Meng. Effect of electromagnetic field on natural convection in inclined porous layer. *J. Heat Transfer and Fluid Flow*, **17**(1): 1996

[2] B. Goyeau, J.P. Songbe, D. Gobin. Numerical study of double-diffusive natural convection in a porous cavity using the Darcy–Brinkman formulation. *Int. J. Heat and Mass Transfer*, **39**(7): 1363–1378, 1996.

[3] S. Ergun. Fluid flow through packed columns. *Chem. Eng. Progr.*, **48**: 89–94, 1952.

[4] S. Kimura, A. Bejan. The boundary layer natural convection regime in a rectangular cavity with uniform heat flux from the side. *J. of Heat Transfer*, **40**: 21–38, 1984.

[5] J.L. Lage. effect of the convective inertia term on Bénard convection in a porous medium. *Numerical Heat Transfer*, Part A, **22**: 469–485, 1992.

[6] G. Lauriat, V. Prasad. Natural convection in a vertical porous cavity: a numerical study of Brinkman-extended Darcy formulation. *Journal of Heat Transfer*, **109**: 688–696, 1985.

[7] G. Lauriat, V. Prasad. Non-Darcian effects on natural convection in a vertical porous enclosure. *Int. J. Heat and Mass Transfer*, **32**: 2135–2148, 1989.

[8] P. Le Breton, J.P. Caltagiron, E. Arquis. Natural convection in a square cavity with thin porous layers on its vertical walls. *J. Heat Transfer*, **113**: 892–898, November 1991.

[9] P. Nithiarasu, K.N. Seetharamu, Sundararajan. Double-diffusive natural convection in an enclosure filled with fluid-saturated porous medium: a generalized non-Darcy approach. *Numerical Heat Transfer, Part A*, **30**: 413–426, 1996.

[10] S.V. Patankar. *Numerical heat transfer and fluid flow.* Hemisphere, McGraw–Hill, New York, 1980.

[11] O. Trevisan, A. Bejan. Natural convection with combined heat and mass transfer effects in a porous medium. *Int. J. Heat and Mass Transfer*, **28**(8): 1597–1611, 1985.